Advances in PPG Sensors Data Acquisition With Light-to-Digital Converters: A Review

Nishan Chettri, *Graduate Student Member, IEEE*, Antonio Aprile, *Member, IEEE*, Edoardo Bonizzoni, *Senior Member, IEEE*, and Piero Malcovati, *Senior Member, IEEE*

***Abstract*—Light-to-digital converters (LDCs) are essential components in photoplethysmography (PPG) readout chains. Over the past decade, PPG sensors have gathered increased interest due to their non-invasiveness and employment in a wide variety of applications. Among these are cardiovascular monitoring, brain mapping, glucose sensing, skin cancer detection, ozone pollutant sensing, and commercial fitness tracking devices. This article offers a review of recent developments in PPG monitoring, with a specific focus on LDCs. The critical challenges, such as light-emitting diode (LED) power consumption, low perfusion index (PI), ambient light interference, and motion artifacts (MAs), are discussed in detail. Different sampling methods (uniform aggressive, compressive, and event-driven) are analyzed to provide an overview of the mitigation techniques of the LED power consumption issue. Moreover, specific circuit solutions to overcome the remaining challenges are explored within the power consumption and signal quality trade space. Recent advances in LDCs employing on-chip photodetectors (PDs) and dc cancellation circuits are discussed as they significantly improve the noise performance of the readout and provide a considerable overall power reduction. The article also evaluates state-of-the-art (SoA) circuit design techniques, providing essential considerations and intuitions. Lastly, it outlines future development trends and insights, charting a course for continued innovation in this rapidly evolving field.**

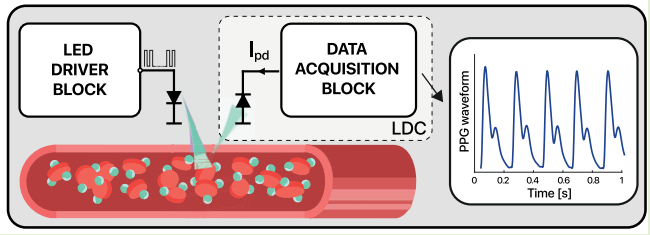

***Index Terms*— Biomedical signal processing, cardiovascular monitoring, light-to-digital-converter (LDC), photoplethysmography (PPG), pulse oximetry.**

I. Introduction

PHOTOPLETHYSMOGRAPHY (PPG) is a noninvasive optical technique that employs light absorption principles to detect volumetric changes in the blood at peripheral circulation during cardiac cycles. It helps distinguish arterial pulsations, offering insights into cardiovascular dynamics, oxygen saturation (SpO^2), and even emotional states [1]. A PPG sensor system comprises a light-emitting diode (LED) driving block, an LED, a photodetector (PD), and a data acquisition block. The driving block controls LEDs to emit specific wavelengths of light that penetrate the skin and tissues; the corresponding photons are either absorbed, scattered, or reflected by the underlying blood vessels, causing variations in the intensity of the reflected light due to changes in blood volume with each heartbeat. The reflected light is converted to a photocurrent by the PD. Lastly, a data acquisition block is employed to perform analog signal processing and convert the photocurrents to digital codes. These digital codes are further processed to obtain raw PPG signals. A simplified interpretation of the components of such a signal is depicted in Fig. 1. It illustrates that the PPG waveform originates from the unabsorbed light detected by the optical sensor or PD. The measured PPG intensity (I) exhibits an inverse correlation with the light absorbance (A) in the volume of tissue under examination. Considering the impact of light absorbance on different segments of tissue, the PPG intensity can be segregated into two components: the non-pulsatile component, characterized as a quasi-static dc component, arises from the absorption of light in non-pulsating tissue regions (e.g., bloodless tissue, muscle, bone, etc.) while the pulsatile component, depicted as the ac component, emerges from the absorption of light in the pulsating arterial blood and fluctuates rhythmically with each heartbeat [2]. The morphology of this waveform is determined by several factors: the heart, the circulatory system, other physiological processes including breathing and the autonomic nervous system, and diseases [3]. Crucial physi-

Manuscript received 29 May 2024; accepted 20 June 2024. Date of publication 3 July 2024; date of current version 15 August 2024. The associate editor coordinating the review of this article and approving it for publication was Dr. Sanjeev Kumar Raghuwanshi. *(Corresponding author: Nishan Chettri.)*

The authors are with the Department of Electrical, Computer and Biomedical Engineering, University of Pavia, 27100 Pavia, Italy (e-mail: nishan.chettri01@universitadipavia.it; antonio.aprile01@universitadipavia.it; edoardo.bonizzoni@unipv.it; piero.malcovati@unipv.it).

Digital Object Identifier 10.1109/JSEN.2024.3420170

© 2024 The Authors. This work is licensed under a Creative Commons Attribution-NonCommercial-NoDerivatives 4.0 License.
For more information, see https://creativecommons.org/licenses/by-nc-nd/4.0/

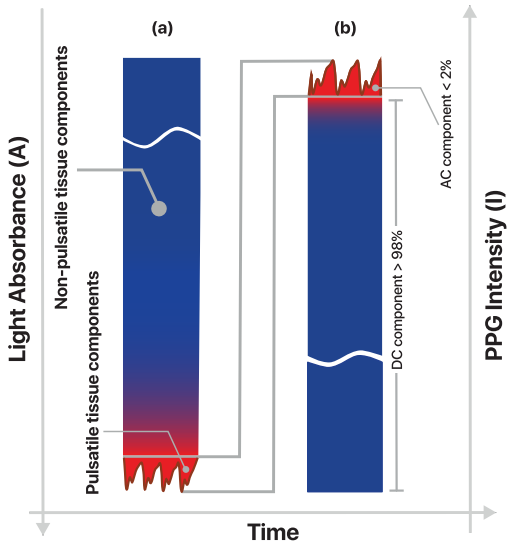

Fig. 1. Conceptual representation of a PPG signal waveform. (a) Light absorbance as a function of time. (b) PPG signal intensity as a function of time.

ological parameters like cardiac ejection, heart rate (HR), heart rhythm, stroke volume, arterial stiffness, blood pressure, and respiration are conveyed into the ac component, which consists of only a small fraction (typically up to 2%) of the whole signal in contrast to the quasi-static one. These insights are primarily obtained using rigorous signal processing and feature extraction algorithms on the digital codes obtained from the light-to-digital-converter (LDC) [4]. In the past decade, there has been widespread interest in PPG sensor systems due to their critical role across various commercial wearable fitness and health monitoring devices, resulting in an exponential increase in research interest to make such systems viable, efficient, and precise.

II. Design Considerations and Challenges

An LDC is a crucial component in PPG sensor systems; from an industry perspective, it is considered as a system that comprises a PD and a data acquisition block, converting incoming light signals to digital codes, irrespective of its application [5], [6], [7]. However, from the point-of-view of PPG sensor systems available in the literature, the term LDC has garnered different shades. According to a review on LDCs by Mohammad et al. [8], it is generically indicated as a circuit that converts photocurrents to a voltage signal. Another interesting review by Ebrahimi and Gosselin [9] compiles the points of view of different PPG sensor works and classifies their readout topologies as LDC and transimpedance amplifier (TIA)-based. To simplify the classification for the prospective reader, this work defines an LDC as a subsystem of a PPG system, including a PD and a data acquisition block converting light signals into digital codes. This definition generalizes the concept, and this work refers to any PPG subsystem in past works that utilizes an LDC. Furthermore, based on the analog signal processing choices of past works, the LDCs are recognized into two simple categories: TIA-based and TIA-less.

As illustrated in Fig. 2, TIA-based LDCs [10], [11], [12], [13], [14] employ a TIA that converts the photocurrents

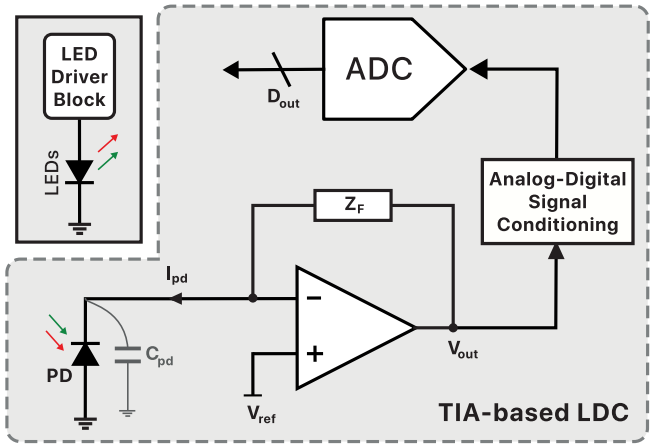

Fig. 2. PPG sensor system with a TIA-based LDC.

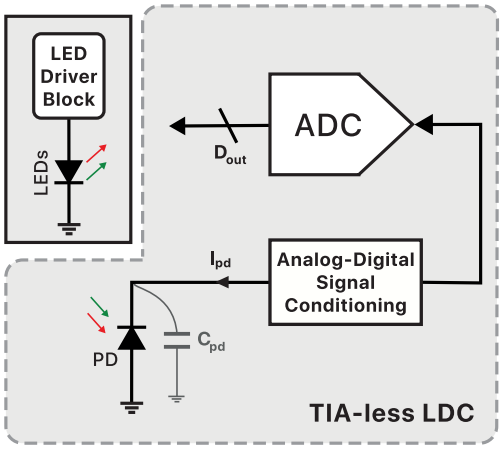

Fig. 3. PPG sensor system with a TIA-less LDC.

collected from the PD to voltage domain signals; the analog-digital signal conditioning (ADSC) block represents the application-specific techniques employed in LDCs in order to tackle the various challenges discussed later in this section. Further, the voltage signal undergoes conversion into digital codes through a voltage-mode analog-to-digital converter (ADC). The gain of the TIA affects the performance of the system as a higher gain corresponds to lower input-referred noise but could saturate the ADC's dynamic range (DR). Considering the pulse repetition frequency (PRF), which is the number of times the LEDs are pulsed every second, lower PRFs can result in increased bandwidth requirements of the TIA, potentially causing problems like noise folding and aliasing [15]. On the other hand, TIA-less LDCs, as illustrated in Fig. 3, do not incorporate a TIA. This class of LDCs have gained popularity as they integrate amplification, filtering, and digitization of PD current in one stage, eliminating the need for a TIA. This approach is well-suited for duty cycling to enhance power efficiency, as it shifts the fast-settling requirement from the TIA to the ADC. This is typically achieved by employing an ADC with a higher conversion rate [16], [17], [18], [19], [20], [21], [22]. Recently, Lin et al. [15] introduced an LDC employing a dual-slope, charge-counting ADC that offers a high DR along with inherent low-pass filtering in the front-end.

In this class of LDCs, some of the works also employ a current-mode approach. Kim and Jee [17] presented a low-power PPG-recording system featuring a distributed, 1-bit delta-sigma ($\Delta\Sigma$) modulator in current mode. However, this system may encounter limitations in DR due to its current self-integration. There are only a handful of works that have employed a current-mode approach for analog sensor data to digital conversion [20], [23], [24], [25], [26], [27], [28] due to limitations in terms of noise, low DR, and nonlinearity.

As introduced earlier, a PPG signal comprises a quasi-static and a pulsatile part. The first is due to the skin, bone, and tissue components at the PPG measurement site, while the latter primarily corresponds to blood volume changes synchronized with each heartbeat. Apart from these, multiple other factors contribute to the variability of a PPG signal: temperature fluctuations [29], LED placement (reflection mode or transmission mode) [30], [31], skin pigmentation and composition, arterial diameter, concentration and direction of oxygenated and deoxygenated hemoglobin [32], [33], [34], and site of measurement [35]. The wavelength employed for the light/tissue interaction is also crucial, given that different wavelengths penetrate tissues in varying depths [36], [37], [38]. Breathing influences the PPG signal by modulating its amplitude, frequency, and baseline drift [39], [40]. Motion artifacts (MAs) require optimal skin contact for optimal quality PPG signals [41]. Thus, it is crucial to take into consideration all of these factors during the design of high-precision sensor systems for cardiovascular measurements.

A. Challenges at Macrolevel

1) Motion Artifacts: MAs arise from alterations in sensor positioning or from changes in the pressure exerted on the skin due to movements in the PPG measurement sites. These artifacts are due to variations in the air gap length between the probe and the tissue during motion, causing fluctuations in the light absorption within the tissue and affecting light scattering and reflection. These artifacts typically manifest as low-frequency (LF) interferences. The occurrence of MAs can be attributed to two primary factors: first, variations in the sensor-skin contact, detectable using additional sensors such as accelerometers and gyroscopes, can be mitigated through data processing. The work by Han et al. [42] introduces a wearable finger band PPG device comprising a three-axis accelerometer, infrared (IR) LED, photodiode, microprocessor, and wireless module. They employ a 2-D active noise cancellation algorithm to mitigate signal distortions caused by motion, utilizing directional accelerometer data. This approach reduces signal distortion rates from 52.34% to 3.53% within the frequency range of 1–2.5 Hz, corresponding to common daily activities like walking and jogging. Second, temporal changes in light scattering from the skin tissues due to shifts in the relative position between the sensor and the skin can result in inconsistent data. In a study by Lee et al. [43], a skin-attachable PPG sensor equipped with an orthogonal polarizer–analyzer (OPA) pair configuration is proposed, which effectively reduces MAs by suppressing the amount of light scattered from the skin epidermis before it reaches the PD. The design resulted in a tenfold reduction in MAs compared to rigid sensors. In this framework, another intrinsic way of addressing this issue is by adopting multiple wavelengths of light and multichannel PPG recording. Zhang et al. [44] utilize a green wavelength PPG signal for HR monitoring, while an IR one is the reference for motion detection. The signal corresponding to green light predominantly reaches the capillary layer, resulting in a higher ratio of ac to dc component compared to the one obtained using IR, which can penetrate deeper. The MAs in the IR PPG signal exhibit a significantly larger amplitude due to a greater change in the light path, in contrast to MAs in the green PPG signal. They report a signal-to-motion ratio (SMR) of at least 10 dB higher in the green PPG signal compared to the IR one. Pandey and Chao [45] also proposed a dual-channel PPG sensor but using OLED and organic photodetectors (OPDs). They employed an LDC with multiple feedback loops to counteract dc drifts resulting from the movement between the sensor and the skin, as well as between the skin and blood vessels. The results demonstrated a significant reduction in MAs, successfully diminishing it from 20% of the average dc drift to a mere 1%. The strategies employed to reduce MA involve trade-offs. The incorporation of additional hardware adds to the form factor and power consumption specifications. Additionally, the complexity and digital processing requirements increase with the inclusion of extensive signal-processing algorithms.

2) Optical Crosstalk: PPG signals are low amplitude signals that maintain a regular pulse frequency within the 0.5–5 Hz range [46]. Optical crosstalk in these signals is caused due to ambient light interference; this results in inaccuracies during the estimation of physiological parameters like HR. Ambient light interference can arise from a plethora of sources, including constant frequency ones like sunlight to variable frequency ones like indoor lighting [47]. The intensity of this interference usually surpasses the pulsatile (ac) component of the PPG waveform by several orders of magnitude, causing signal saturation. Hence, the rejection of ambient light components from the PPG signal holds significance in ensuring the data integrity from PPG sensors [48]. There have been several works aiming to mitigate this problem employing techniques like optical shielding [49], flexible PPG sensors [50], and the employment of an adaptive dc rejection loop [20], [51]; these solutions are implemented along with several digital signal processing (DSP) techniques that have proven to be effective in mitigating optical crosstalk [4], [52]. Some other techniques are discussed in Section III.

3) Biological Differences: The PPG signal acquisition is also dependent on the type of tissue under the measurement site. The nature of tissue type depends on body fat percentage, melanin content on the skin, skin temperatures, ethnicity, and age, which affects the prospective PPG signal. For instance, it was observed that the diastolic peak in young subjects diminishes with age [29], [53], [54], [55]. Advancements such as the utilization of multiple wavelengths and enhancements in device fit aim to mitigate biases. However, the limited publicly accessible data on long-term efficacy and the rapid pace of technological advancements present significant challenges for researchers striving to keep pace. All these external factors

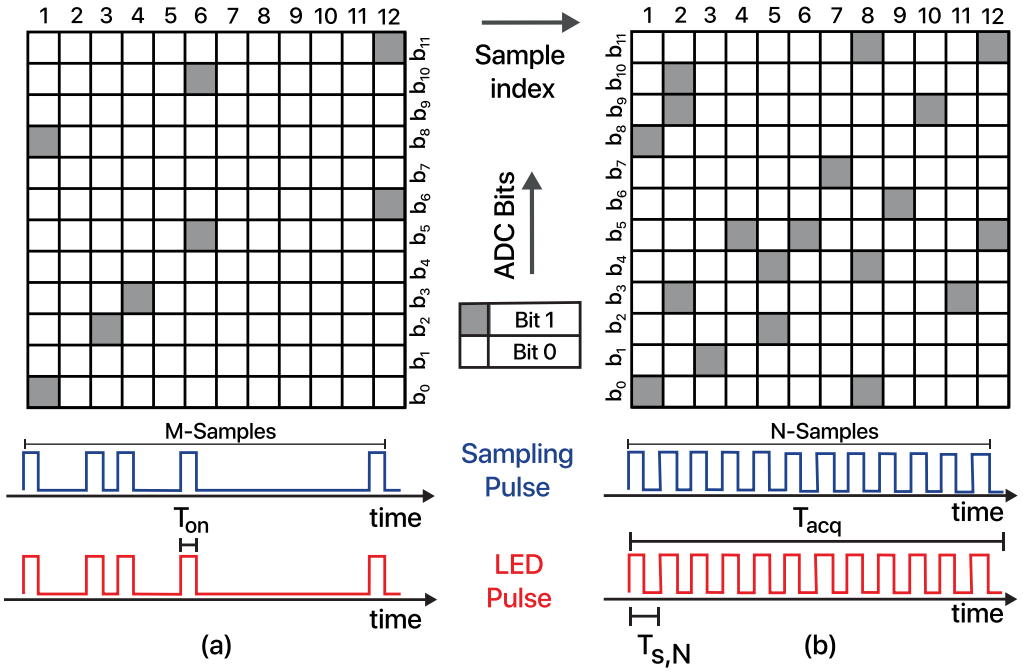

Fig. 4. Measurement matrix structure [56]. (a) Compressive sampling (CS). (b) Uniform-aggressive sampling.

make the design of PPG sensor systems and LDCs, in particular, a multidimensional problem.

B. Challenges at Microlevel

1) Power Consumption of LEDs and Driving Block: Low power consumption is a critical requirement for wearable devices, given their reliance on battery power. Optical PPG is often power-hungry due to the presence of LEDs that need to be driven continuously. There are several techniques that aim to minimize the power consumption of the LEDs like uniform aggressive duty cycling [9], compressive duty cycling [56], and event-driven duty cycling [11], [57]. The uniform aggressive duty-cycling technique is very common among state-of-the-art (SoA) works due to its simplicity but imposes fast settling requirements on the LDC [58]. Bishop et al. [58] introduced an interesting PPG sensing model that showcases the trade-offs in terms of power consumption, signal quality, and circuit design comparing duty-cycled and non-duty-cycled operation of self-powered PPG operation. They illustrate that at lower TIA bias currents, both duty-cycled and non-duty-cycled channels require comparable power levels for the sampling rate being primarily dominated by the consumption due to LEDs. Additionally, each sampling rate corresponds to a distinct minimum power point, with the non-duty-cycled channel exhibiting lower minimum power points only at lower biasing currents compared to duty-cycled channels, which maintain similar minimum power points across the swept biasing currents. The discussed architecture in the model illustrates that with an increase in bias current, the SNR decreases; as a result, the minimum power condition of the duty-cycled channel is achieved at higher bias currents with respect to the non-duty-cycled one. The lower bias point condition might seem appealing, but comes at the cost of reduced signal swing at the LDC input, increasing the design complexity.

Another category of sampling scheme employed to potentially reduce the power consumption of PPG sensor systems is CS. Fig. 4(a) and (b) represents a partial measurement matrix structure for a PPG sensor system employing CS and conventional uniform-aggressive sampling, respectively. The sampling index is indicated from left to right, while the output bits of a 12-bit ADC are indicated with respect to the sampling pulse and the LED pulse. In the CS approach, specific signal classes can be accurately reconstructed using significantly fewer samples than those required by conventional uniform aggressive sampling methods [56], [59]. As evident in Fig. 4, only a few sample indices have the respective ADC bits sampled according to the compression ratio (CR) given by M/N; M and N represent the number of samples taken for CS and uniform aggressive sampling, respectively. On the contrary, in the case of Fig. (b), the signal is sampled at every index. For example, at index 8, the 12-bit ADC in (a) outputs all zeros, whereas in case of (b), the output is 0×881. Defining $f_{s,\mathrm{US}}$ as the sampling frequency for the uniform aggressive case and $f_{s,\mathrm{CS}}$ as the sampling frequency for the CS case, the following relationship holds:

$$f_{s,\mathrm{CS}} = \frac{f_{s,\mathrm{US}}}{\mathrm{CR}}. \tag{1}$$

Pamula et al. [56] performed an in vivo acquisition of PPG signals, employing both uniform sampling mode and CS with CRs of $8\times$, $10\times$, and $30\times$. It was measured that the LED power consumption scales from 1200 to 43 μW when a CR of 30 was employed. While CS offers competitive advantages in terms of reducing power consumption, it also introduces complexities in the system, particularly during the reconstruction of the sampled data. In fact, the power consumption of the ASIC was mainly dominated by the LDC, which consumed 172 μW. Additionally, as the CR is increased

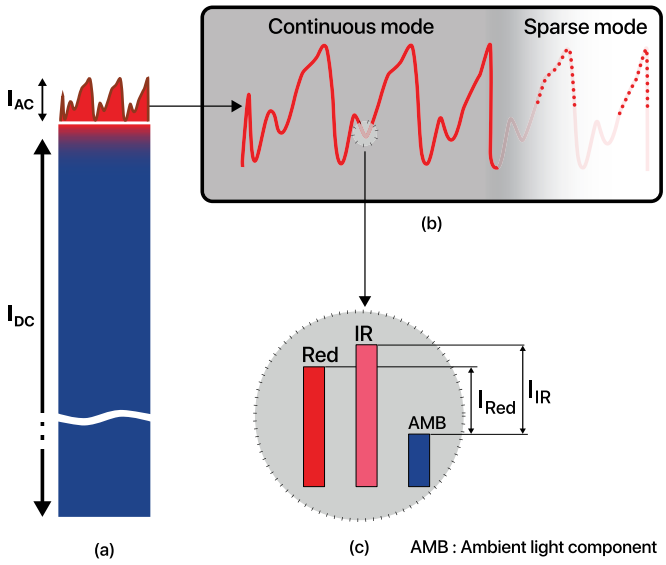

Fig. 5. (a) PPG signal ac and dc components. (b) Event-driven sparse sampling algorithm. (c) Red and IR signals.

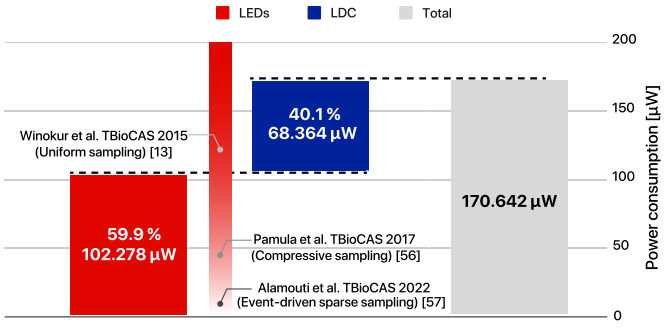

Fig. 6. Average power consumption of PPG sensor system blocks from prior works.

from 10 to 30, the decrease in LED power consumption comes at the cost of an increase in HR error from 2 to 10 bpm. Another interesting approach is the event-driven sampling method employed in the work by Alamouti et al. [57]. It outperforms both the previously discussed techniques in terms of LED power consumption. Fig. 5(a) represents a PPG waveform with its ac and dc components on which a sparse sampling algorithm is employed as seen in Fig. 5(b); Fig. 5(c), instead, shows that, after subtracting the ambient light component sample represented as AMB, processing on different wavelengths of illuminated light is performed by means of system-level correlated double sampling (CDS). This process specifically depends on identifying only a minimal number of samples with an observation window centered around the peaks and valleys (PAVs) of the collected waveform. Initially, the on-chip algorithm performs uniform sampling at a rate of 100 Hz, known as continuous mode. Afterward, the sensor transitions to sparse mode, during which sampling is exclusively carried out around the predicted PAV locations as depicted in Fig. 5(b). Through this approach, the total sample count required for extracting SpO^2 and HR is reduced by approximately 4×, resulting in an overall power reduction of around 70%. Reduced power consumption is accomplished by implementing a smaller window size; however, during notable MAs, if the window size is not large enough, it poses a risk of recurrent missed PAV detections, thereby causing HR error. To address this issue, the DBE enlarges the observation window until new PAVs are identified. If, despite reaching the maximum window size, no new PAVs are detected, the system reverts to the initial phase [57]. The requirement of a complex reconstruction algorithm and scheme makes this technique less favored. Fig. 6 consolidates the average power consumption from SoA works [10], [11], [13], [14], [15], [16], [17], [19], [20], [21], [22], [24], [56], [57], [60], [61], [62], [63], [64], [65], [66], [67], [68], [69] over the past decade. It is clear that the LEDs and their driving blocks are responsible for approximately 60% of the total power consumption in PPG systems. Moreover, Fig. 6 depicts the performance of three distinct works utilizing different sampling techniques to address the LED power consumption problem. Considering the present SoA works, the event-driven sampling method clearly outperforms the other techniques in mitigating this issue.

2) Low Perfusion Index: Perfusion index (PI), as shown in (2), is the ratio between the pulsatile (ac) and the quasi-static (dc) component of a PPG signal

$$\mathrm{PI} = \frac{\mathrm{ac}}{\mathrm{dc}}. \tag{2}$$

The challenges due to low PI are multifaceted and demand innovative solutions for accurate monitoring in various wearable devices. PPG sensors have a PI typically ranging from 1% to 4% when placed on fingers. This translates to a DR requirement of at least 65 dB to precisely record HR. The PI value differs depending on the positioning of the sensors and the distribution of blood vessels in the measurement site [70]. In the work by Du et al. [71], single channel and dual channel PPG measurements were performed and it was observed that the center of the forehead had lower PI than the surrounding area. The inclusion of additional channels effectively increased the sampling area of the sensor, thus reducing the amount of error both between measurements at the same site and across different measured sites on the same person [71]. Similarly, on the wrist where the PI diminishes to 0.05%–1%, achieving reliable HR records demands a DR higher than 80 dB while for SpO^2 monitoring the required DR even exceeds 90 dB [11], [72], [73]. Hence, the microlevel challenges impose exorbitant DR requirements of around 120 dB on the ADC used in the data acquisition chain of the LDC. Most of the studies employ an external PD with an additional dc cancellation circuitry to mitigate this issue. Alternatively, the work by Caizzone et al. [65], [74] demonstrates the feasibility of a PPG sensor through device-level modifications aided by the implementation of on-chip pinned photodiodes (PPDs). Their approach utilized a double transfer gate (TG) structure, depicted in Fig. 7(a). This structure comprises two TGs: a charge sink TG (TGs) and a charge transfer TG (TGt). The PPD structure comprises a p-n junction buried beneath a thin layer of heavily doped p+ material, functioning like a charge well [74]. The control of the charge accumulated in the well is enabled by the two gates and detected through the sense node (SN). The device operates through three fundamental phases,

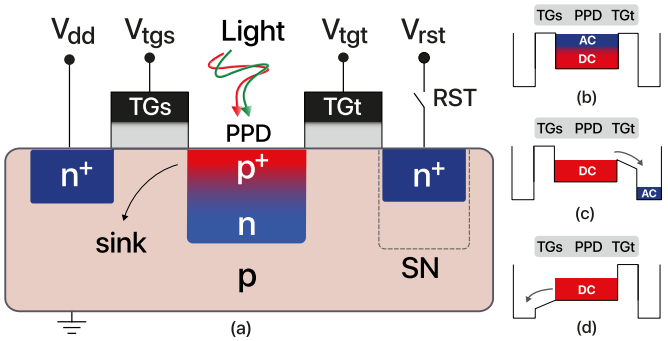

Fig. 7. (a) PPD device employing a dual-TG structure and its working phases. (b) Integration phase. (c) PI enhancement phase. (d) Sink phase [74].

as depicted in Fig. 7(b)–(d): integration, PI enhancement, and sink phases. During the integration phase, both ac and dc components of the PPG signal are integrated into the charge well. Subsequently, only the ac component of the signal is transferred from the well by adjusting the barrier potential using TGt during the PI enhancement phase. This leaves the dc component in the well, which is then reset using TGs in the sink phase. Through this method, Caizzone et al. [65] achieved an ultralow-power LDC with a remarkably low power consumption of only 2.63 μW.

III. Building Blocks and Design Techniques

As mentioned above, an LDC is the part of a PPG sensor system that includes the PD and the data acquisition block. The obtained digital codes (D_{out}) undergo a series of signal processing steps: pre-processing, identifying individual pulse waves, extracting pulse wave features, estimating physiological parameters, and developing models to obtain end-user relevant information for various wearable medical and fitness device applications [4]. In turn, an LDC is comprised of many building blocks, namely optical reception block, TIA, ADSC, and ADC. These blocks, along with their main state-of-art design techniques, are discussed in detail in this section.

A. Optical Reception Block

In LDCs, LEDs emit pulsed light to illuminate various human tissues where a portion of the light is absorbed, another part is scattered, and the rest is reflected toward the PD. Typically, the LEDs are turned on for a duration ranging from 0.0125% [10], [56] to 10% [17] of their full period. A PD detects the reflected light from the tissues and transforms it into a photocurrent, as shown in Figs. 2 and 3. An LDC system inherits several problems from the PD. One of them concerns the parasitic capacitance (C_{pd}) that directly influences signal-to-noise ratio (SNR) and power consumption. Equation (3) provides an analytical expression of C_{pd} [14], where ϵ_{Si} is the silicon dielectric constant, A_0 is the junction area, μ_0 is the mobility of electrons, ρ_0 is the silicon resistivity, V_{bi} is the built-in voltage, and V_{pd} is the bias voltage of PD

$$C_{\text{pd}} = \frac{\epsilon_{Si} \cdot \epsilon_0 \cdot A_0}{\sqrt{2 \cdot \epsilon_{\text{Si}} \cdot \epsilon_0 \cdot \mu_0 \cdot \rho_0 \cdot (V_{bi} + V_{\text{pd}})}}. \tag{3}$$

The size of the PD directly influences the LDC system as a larger junction area results in a larger C_{pd}. The cost to obtain the same SNR with a PD having larger C_{pd} is paid with increased power consumption [75]. The intuition behind this trade-off comes from the allowed minimum pulsewidth of the LEDs (T_{on}) that directly affects the total system power consumption (P_{tot}). Reducing C_{pd} allows for a shorter T_{on}, leading to a lower P_{tot}. A larger C_{pd} confines the T_{on} to a higher value to achieve the same SNR. Equation (3) highlights two approaches for reducing C_{pd}: scaling down the physical size of the PD or, from a circuit perspective, applying a dc bias voltage directly to the PD itself (other parameters in (3) are all technology dependent). Furthermore, the bias voltage affects the PD's capacitance in on-chip integration; therefore, careful selection of bias voltage and optimization of biasing circuits are essential to ensure the PD operates efficiently.

Another problem typically faced is LF noise due to ambient light interference. This can be reduced dramatically by techniques like CDS where the ambient light is sampled and then subtracted from the signal [75], [76]. If the time between the two samples is comparable to the on-time (T_{on}) of the illuminated LEDs, an almost ambient-free PPG signal is obtained [75]. Integration of the input photocurrent is another way of reducing the effect of wide-band noise [15]. Recent advances suggest that the integration of the PD on-chip results in a significant reduction in the total power consumption from hundreds of μW to tens of μW as seen in the work by Caizzone et al. [65] that resulted in a benchmark-low P_{tot} of 4.6 μW with the LEDs consuming a meager 2 μW. This was possible due to the high sensitivity quantum efficiency (QE) of the on-chip CMOS PPDs described in Section II-B, enabling their operation in low-light conditions and requiring lower illumination from the LEDs. However, in low-light scenarios, electronic temporal readout noise (TRN) dominates the overall noise. Under moderate illumination, instead, the SNR is proportional to the number of photoelectrons (N) as photon shot noise (PSN) becomes the primary noise factor [75], [76]. Lastly, at high levels of illumination, fixed pattern noise (FPN) arising from inconsistencies between PPD pixels restricts the SNR [77]. Hence, the design of low-noise circuits for the LDC is critical to fully capitalize on the sensitivity of PPDs. Another interesting work by Kim and Jee [17] proposed an integrated array of 128 $\times$ 64 μm p-n diodes where each pixel of the array employs a dedicated local 1-bit Δ-Σ modulator. This distributed architecture achieved a low equivalent noise of the order of 20.4 pA_{rms}, approximately 10 dB lower than traditional designs, resulting in an improved DR and total power consumption of less than 25 μW.

B. Transimpedance Amplifier

As addressed earlier, the magnitude of the pulsatile component of the photocurrent is very small compared to the quasi-static dc one, hence requiring amplification before it is quantized and converted to digital codes. Moreover, in many cases, when the quantizer is a voltage-mode ADC, the photocurrent has to be converted to an amplified voltage signal. This current-to-voltage conversion is performed by one of the most influential blocks of an LDC, i.e., the TIA, whose

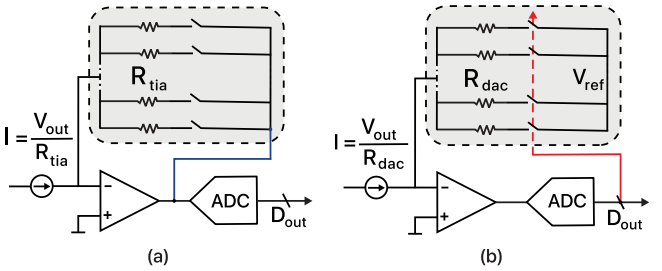

Fig. 8. Comparison of conventional class of (a) TIAs with (b) digitally assisted one [68].

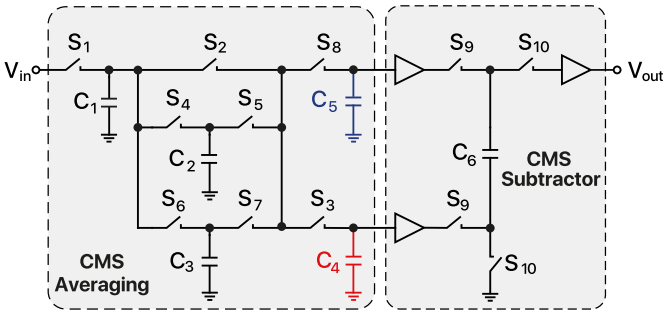

Fig. 9. Eighth-order passive SC CMS implementation [81].

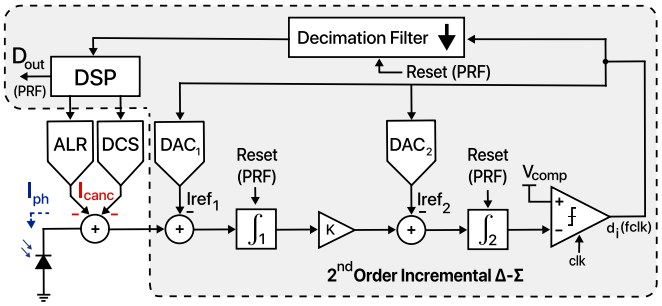

Fig. 10. Digitally assisted LDC based on a second-order incremental ADC for signal-aware dc subtraction (DCS) and ambient light removal [20].

stability, noise, and bandwidth directly influence the performance of TIA-based LDCs [2]. To minimize the power consumption of a PPG system, various duty-cycling techniques on the LEDs are used. Consequently, the TIA has to be fast enough to settle within a short interval of time; from a design viewpoint, the signal power is distributed over a very large number of harmonics, increasing the bandwidth required to recover it [9], [11], [56], [78].

There are three classes of TIAs commonly employed in the literature, distinguished mainly due to the nature of feedback they use, namely resistive, capacitive, and RC. Resistive TIAs used in recent LDCs have shown the necessity for a very high-value feedback resistor (R_f) costing larger area and thermal noise [60], [61], [62]. In comparison, the capacitive ones provide 10× better SNR for the same gain [75]. As mentioned before, power consumption due to LEDs is another challenge that plagues PPG systems, and often, aggressive duty-cycling is performed to address this issue, setting very stringent settling time requirements on the TIA; its output voltage should be able to settle within the ON-time (T_{on}) of the LEDs, imposing a large bandwidth and slew-rate requirements on the TIA itself [9], [75]. RC-TIAs are spotted to perform better in terms of power consumption for the same bandwidth; it has been noticed that they need 8× less LED power than capacitive TIAs to achieve the same SNR at a given bandwidth [75]. In addition, they also minimize the effect of C_{pd} on the overall noise [56].

In traditional TIAs, the choice of the gain involves a compromise between minimizing input-referred noise and maximizing input range. As shown in Fig. 8, the work by Shu et al. [68] employs a digitally assisted one to mitigate this problem by incorporating a resistive 11-bit DAC in the feedback path with a dynamic element matching (DEM) technique to achieve better linearity. As a result, the TIA gain becomes considerably large, helping input-referred noise suppression. Moreover, in the same work, DSP techniques are used to further process the digital data, achieving a remarkable DR of 130 dB across the PPG bandwidth while operating at a duty cycle of 0.625% and 72 μW of power consumption.

C. Analog-Digital Signal Conditioning

The AFE4400 pulse oximeter [79] offers one of the most straightforward ways of recording a PPG signal by using an ADC with a very high DR. The limitation of this approach is that most of the DR is used to quantify the dc part of the signal, costing power. Other studies have employed various methods to improve the power efficiency of such a system. The ADSC block, illustrated both in Figs. 2 and 3, generalizes all the techniques utilized in LDCs. One particularly effective method in enhancing thermal and $1/f$ noise performance is correlated multiple sampling (CMS); as seen in the research conducted by Capoccia et al. [80], both theoretical estimation and experimental verification of the work demonstrated a 33% reduction in $1/f$ noise in CMOS image sensor (CIS) readout chains that integrated two distinct pixels. This integration featured a variable gain column-level amplifier (CLA) and an eighth-order passive switched-capacitor (SC) CMS circuit. Fig. 9 illustrates a typical eighth-order CMS stage employing a passive SC implementation. The circuit comprises a stage that averages the input signal and ambient light information at two distinct time points and samples them across separate capacitors, namely C_4 and C_5. The CMS subtractor then computes the difference between these two averaged values [81]. This technique effectively mitigates LF noise caused by ambient light interference [75], [76].

DC subtraction (DCS) is another technique widely employed for the cancellation of the dc component of the signal before it is digitized, allowing for an optimized use of the full-scale input range of the ADC. Fig. 10 illustrates re-configurable current DACs used within an LDC based on a second-order incremental $\Delta\Sigma$ ADC [20]. This system executes three distinct phases: DCS, ambient light rejection (ALR), and signal measurement. During the DCS phase, the first current branch of the reference DACs is engaged, establishing a 51.2-μA input full-scale. This phase involves a dual-step process: measuring ambient light (10-bit) with the LED OFF, followed by a 10-bit measurement of PD current (I_{ph}) when the LED is active. The DSP unit differentiates these values, isolating the dc component of the signal. Subsequently,

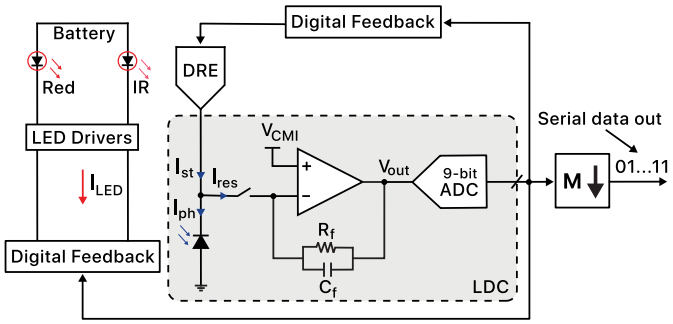

Fig. 11. Simplified block diagram of the PPG SoC work by Winokur et al. [13].

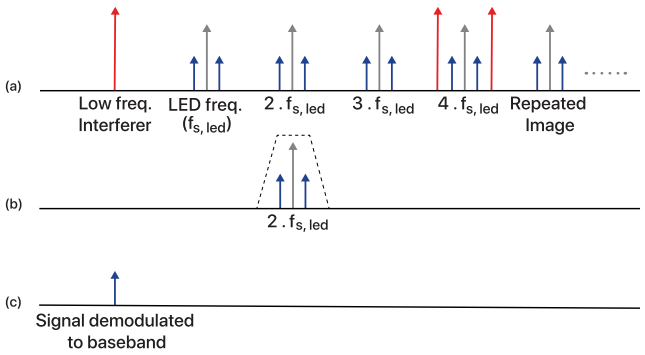

Fig. 12. Time-varying interference removal algorithm. (a) Frequency-domain representation of signal and interferer. (b) Filtering around the second modulated image of the signal to remove unwanted interference. (c) Demodulation by decimation for obtaining a clean signal at baseband [13].

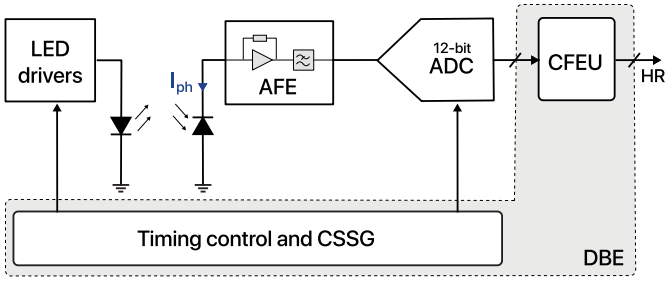

HR: Heart Rate , CSSG : Compressive Sampling Control Generator
DBE : Digital Backend , CFEU : Control and Feature Extraction Unit

Fig. 13. System-level representation of a compressively sampled LDC [56].

a user-defined percentage of this dc component is programmed into the DCS DAC. The DCS phase operates on a 10-s cycle, allowing for the averaging of dc values over eight successive measurements to enhance resolution. In the ALR phase, the second current branch of the reference DACs is activated, adjusting the input full-scale to 25.6 μA. Ambient light is measured (10-bit) 50 μs prior to each signal-measurement phase, with the corresponding 10-bit code programmed into the ALR DAC by the DSP unit. The signal measurement phase involves activating the third current branch of the reference DACs, setting the input full-scale to 0.4–12.8 μA (5 bits). During this phase, the LDC operates with a 13-bit resolution at a 4-ms interval (PRF of 250 Hz). The LED is illuminated for 128 μs, and preprogrammed DCS/ALR DACs inject currents to dynamically cancel the latest dc and ambient light-induced components in the PD. This intricate process ensures accurate and real-time signal measurement in challenging ambient conditions. The challenges at the macrolevel concerning PPG sensor systems highlight the significance of power consumption attributed to LEDs and driving blocks as a critical bottleneck in their design. Uniform aggressive duty cycling, as described earlier, is a straightforward method to reduce the power consumption of the LED driving block by decreasing the turn-on period of the LEDs.

A system-level representation of the work by Winokur et al. [13] is illustrated in Fig. 11, where the driving current is optimized by a digital feedback algorithm. According to the digital output code, the LED drivers modulate the LEDs to increase the energy efficiency of the system. A duty cycle of 0.7% is used, which corresponds to a square LED current pulse that is 40 μs wide every 6.06 ms. In addition to the low-power digital feedback technique, a low-power removal of time-varying interferers by using modulation, filtering, and decimation is proposed to enhance the DR of the overall system; its resulting frequency-domain representation is illustrated in Fig. 12. The architecture first involves sampling the output of the PD when the LEDs are ON, as well as when the LEDs are OFF. The signal is sampled at integral multiples of f_s when the LEDs are ON and at $4 \times f_s$ when the LEDs are OFF. The superimposed signal is then filtered and demodulated, after which the signal component returns to the baseband; accordingly, the LF artifacts move beyond the filter stopband, achieving an attenuation of 80 dB or greater in the entire stopband while negligibly increasing the power budget. Nevertheless, the minimum reported power consumption of 120 μW is observed to be higher than the average one of SoA works (Fig. 6). Fig. 13 illustrates the system-level representation of an unconventional work by Pamula et al. [56] using a CS technique as described earlier. This implementation comprises a readout and signal processing chain, which is interfaced with an off-chip PD. Moreover, the work employs CS for reducing the LED driver power consumption and also embeds a low-power digital back end (DBE). This block is capable of extracting the HR information directly from the CS PPG signal by the use of a least square spectral fitting method removing the need for complex reconstruction techniques. This incurs a minimal power penalty of only 7.2 μW, enabling the reduction of LED driver power consumption by a factor of the CR introduced in (1). It is evident from Fig. 6 that this work achieves a power consumption which is better than the average of the considered SoA works.

D. Analog-to-Digital Converters

ADCs are one of the crucial blocks in the process of light-to-digital conversion. Surprisingly, in LDCs, all the varieties of ADCs have not been explored yet, with works mostly limited to the use of $\Sigma\Delta$ and SAR ADC variants. Fig. 14 illustrates the ADCs used in LDC works of the last decade. It is observed that for resolutions up to 15-bit, SAR ADCs are popular due to their low-power nature, while for higher resolutions, $\Sigma\Delta$ ADCs are preferred. Some works have also explored dual-slope [15], [22] and triple-slope [24], [67] converters,

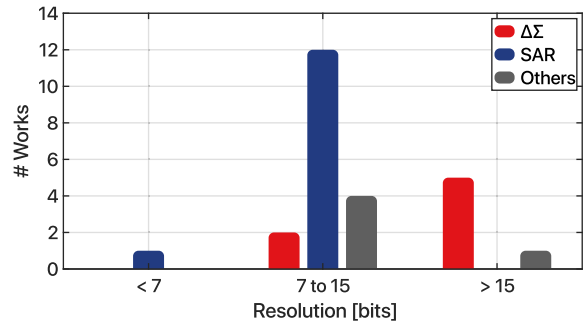

Fig. 14. Number of works as a function of resolution for various types of ADCs used in LDCs.

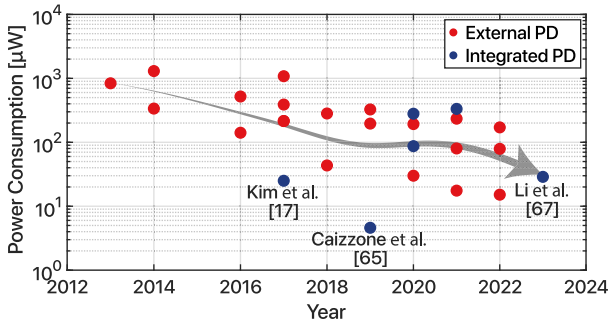

Fig. 15. SoA power consumption in PPG sensor systems as a function of publication year classified on the basis of external and integrated PD.

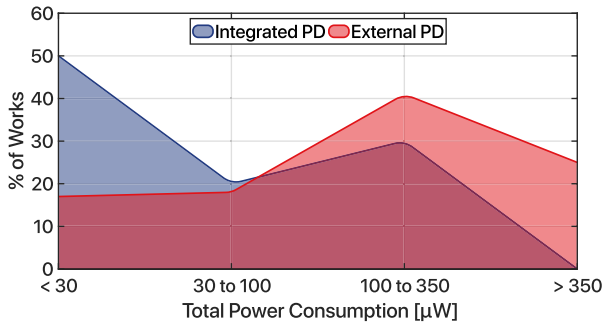

Fig. 16. Total power consumption performance distribution with integrated or external PD distinction.

TABLE I
COMPARISON OF POWER CONSUMPTION DUE TO LDCS WITH INTEGRATED/EXTERNAL PD

LDC Power Consumption	Integrated PD	External PD
Mean	17.2 μW	100 μW
Standard Deviation	12.6 μW	102.3 μW
Minimum	2.6 μW [65]	3.8 μW [57]
Maximum	25 μW [17]	440 μW [12]

which provide high resolutions at the cost of power consumption, complexity, and conversion time. In oversampling converters, like ΣΔ ones, high resolution and low noise are associated with a very high oversampling ratio (OSR), costing higher digital power consumption [20]. To achieve a lower quantization noise with a lower OSR, either the quantizer needs to be of intrinsically higher resolution or multiple integrators must be embedded within the ΣΔ loop [82]. Either of these choices costs power and complexity. Another key architecture that has emerged to strike a balance between the OSR and resolution is the noise-shaping (NS)-SAR ADC architecture [26], [27], [83], [84]. The intuition behind such a converter revolves around the notion of accumulating the residual error achieved after the execution of a successive approximation algorithm and then subtracting it from the input during the subsequent conversion cycle. This process inherently entails a one-conversion delay between the input and the feedback output while alleviating the need for a high OSR to achieve low-noise conditions. Another variant of ADC that is getting popular due to its hybrid and low-power nature is the incremental ADC. It is similar to a ΣΔ converter but with a reset at the end of the conversion period.

Marefat et al. [19] recently introduced an LDC utilizing a first-order, continuous-time, incremental delta–sigma modulator (I–ΔΣM). This design harnesses the specific capabilities of an I–ΔΣM for signal-aware DCS and ALR prior to digitization, optimizing the full-scale input range efficiency in PPG recording. However, a significant drawback of this design is its high duty-cycling level (approximately 10%), resulting in considerable power dissipation of 1.95 mW due to LEDs, despite the LDC's ultralow power consumption of around 8 μW. This is because a first-order I–ΔΣM requires a higher OSR with an extended conversion time to achieve a larger DR; this leads to a longer LED on time (higher duty-cycling level), accounting for the power consumption due to LEDs. The same group proposed an LDC based on a second-order I–ΔΣM [20] as depicted in Fig. 10. This advancement led to a substantial decrease in the system's duty cycle from 10.24% (at a PRF of 100 Hz) to 3.2% (at a PRF of 250 Hz). The decrease in the LED duty cycling directly translates into a remarkable 86% reduction in power consumption of the LED (and its driver), dropping from 1.95 mW to 264 μW during the PPG-recording experiment while maintaining identical DR. The presence of a higher-order I–ΔΣM allows for faster conversion as it requires a lower OSR for achieving the same DR. However, this comes at the cost of an increase in power consumption of the LDC by 7.6 μW (rising from 8.1 to 15.7 μW) due to the presence of an additional integrating stage. Nevertheless, increasing the order remains highly favorable from a holistic, system-level power consumption viewpoint, as LED power is the dominating power consumption source.

Lin et al. [15] proposed a dual-slope charge counting ADC-based LDC utilizing a multifunction integrator to convert the signal current into a voltage while simultaneously serving as a low-pass filter to mitigate the noise folding effect. This integrator also fulfills the sample/hold function during data conversion, thereby reducing the number of noise sources effectively. They were able to achieve a DR of 119 dB with a low power consumption due to LEDs of 107 μW. Nevertheless, this architecture faces a fundamental limitation: achieving high-resolution requires a prolonged conversion time, making it unsuitable for high-bandwidth capacitive micromachined readout scenarios. Additionally, in such a multibit system, thermal noise is likely to be the dominant in-band noise contribution due to the relatively small quantization noise that is effectively shaped out of the band. Conversely, reducing thermal noise requires oversampling, necessitating more efficient, and effective noise reduction methods.

TABLE II
SoA Comparison (Works Reported in Chronological Order)

	Technology [nm]	Duty Cycle [%]	Dynamic Range [dB]	LED Power [μW]	Total Power [μW]	Total Area [mm^2]	ADC Type	Resolution [bits]
[13] TBioCAS 2014	180	0.7	–	120	336.6	3.38[a]	SAR	9
[63] ISSCC 2016	180	2	–	54	141	8.22[a]	SAR	10
[86] ISSCC 2016	250	–	87	–	520	37.7[a]	ΣΔ	15
[12] JSSC 2016	55	8	–	8310	8750	2[a]	ΣΔ	13
[11] JSSC 2017	130	1	97	320	389	5.51[a]	SAR	14
[56] TBioCAS 2017	180	0.0125	–	43	215	10[a]	SAR	12
[10] CICC 2017	130	1.7	112	5500	5537	2.5[a]	SAR	14
[17] ESSCIRC 2017	180	10	113	–	25	1.79[b]	ΣΔ	18
[60] ISSCC 2018	65	1	87	–	282	16[a]	SAR	12
[65] ISSCC 2019	180	0.07	–	1.97	4.6	20[b]	Incremental	14
[22] VLSI 2019	180	0.4	119	107	196	7[a]	Dual Slope	12
[14] TBioCAS 2019	55	0.67	111	205	326	8.66[a]	SAR	13
[68] ISSCC 2020	180	0.625	130	120.6	192.6	4.5[a]	SAR	14
[15] TBioCAS 2020	180	1	95	26	87	7[a]	Dual Slope	12
[20] TBioCAS 2020	180	3.2	108.2	264	297.7	6.9[a]	Incremental	13
[62] JSSC 2021	65	0.5	92	8.5	17.53	4.96[a]	SAR	6
[64] JSEN 2021	350	0.5	–	29.3	80.1	3.91[a]	SAR	12
[87] ISSCC 2021	180	0.04	–	–	25 + LED	1.79[b]	–	12
[16] TBioCAS 2021	180	1	134	305	333	8.37[a]	Dual Slope	10
[61] JSEN 2022	180	0.125	115	47	79	6[a]	SAR	10
[66] BioCAS 2022	180	0.625	119	154	171	4.5[a]	ΣΔ	12
[57] TBioCAS 2022	40	0.25	–	11.4	15.15	2.43[a]	SAR	12
[67] CICC 2023	55	–	136.5	198	228	4.6[a]	Triple Slope	15

[a]Off-chip PD, [b]On-chip PD

An intriguing observation from the two aforementioned studies is that Marefat et al. [20] utilize a broader LED pulse with a lower PRF of 250 Hz, enabling multiple samples to be taken within one period, whereas Lin et al. [15] employ a shorter LED pulse with a higher PRF of 512 Hz, but take only a single sample. The former adopts a second-order incremental delta–sigma modulator (I–ΔΣM) with a 1-bit quantizer. The single-bit quantizer forces the ADC to sample multiple times in a longer pulse repetition period (PRP) to achieve a 10-bit ADC resolution. In contrast, the latter study on dual-slope ADC utilizes higher counting resolution to achieve a large DR exceeding 115 dB despite using a higher PRF.

There are other types of ADCs unexplored for LDC applications, like the SAR-assisted incremental zoom ADC [85] that achieves a high DR for a comparatively low power and area footprint compared to the ΣΔ one. Current-mode variants of ADCs [26], [27] are another candidate that opens up a different approach to LDCs as they alleviate the need for a power-hungry input buffer and a TIA. They are a potentially attractive solution in TIA-less variants of LDCs where the processing has to be done in the current mode.

IV. Comparison and Trends

Recent advances in PPG sensor systems illustrate an obvious trend toward lower power consumption, given its application in battery-powered wearables. Fig. 15 presents an analysis of power consumption based on works published in the past decade, which are categorized depending on whether the LDC has an integrated PD or an external one; the visible trend-line was derived as in [88]. The work by Caizzone et al. [65] serves as a benchmark for power consumption, having achieved the lowest reported value through the utilization of ADSC techniques like CDS and PD integration. Other works [17] and [67], by employing an on-chip PD, also reported relatively low power consumption as compared to the ones following an off-chip approach. Fig. 16 illustrates the percentage of works featuring various levels of total power consumption depending on the employment of integrated PDs or external PDs. It is evident that for sub-30-μW operation, the on-chip approach is more viable, while for more than 30 μW, the off-chip approach is a straightforward option. The on-chip integration of the PD eliminates the need for high-power preamplification circuits, enabling more efficient and scalable SoC designs. Additionally, the use of mature CIS technology enhances sensor power efficiency [69].

Table I shows the power consumption due to LDCs for the on-chip PD solution in comparison with the off-chip one. It is observed that the on-chip approaches have achieved sub-30-μW power consumption, outperforming the off-chip ones. However, this statistic could evolve over time as, at the moment, there are only a handful of works. On the other hand, the limited DR (<90 dB) and the poor spectral responsiveness make this approach challenging. The off-chip approaches that have achieved a comparable total power are the ones that used CS and event-driven duty-cycling techniques as described in Section II-B1. The above-mentioned trend from Fig. 15 provides a direction toward a low-power operation, showcasing that an on-chip PD approach with a low-noise ADSC block is advisable.

Fig. 17(a) depicts a spider chart derived from the average performance values of the works under consideration. This confirms the intuition that for lower power consumption and lower noise, the integrated approach is a plausible solution: these results are enabled by the high QE and CMOS compatibility of the PPDs. Jung et al. [87] demonstrated a PPG sensor module with a form factor of 18.13 mm^2, which is highly desirable considering the wearable consumer electronics framework. This provides an insight that if a PPG sensor

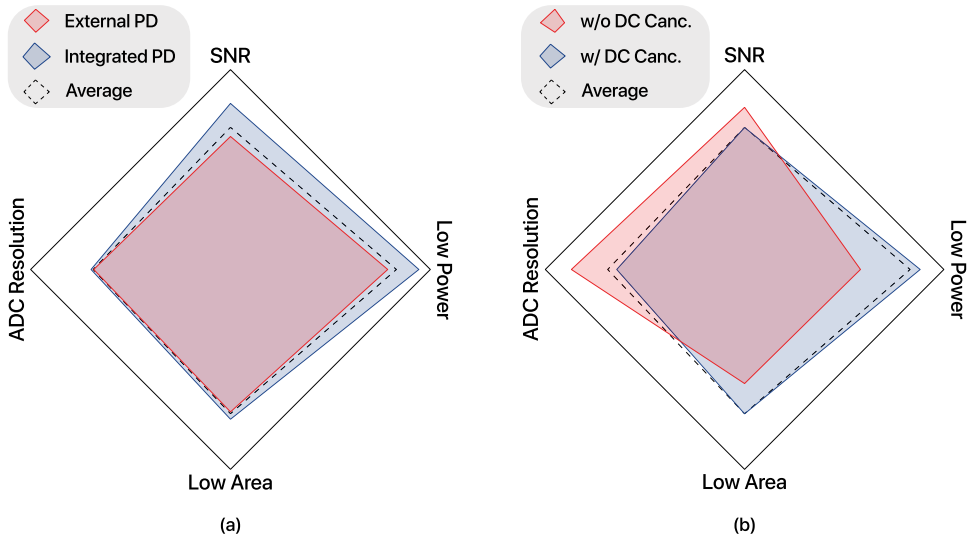

Fig. 17. Spider chart summarizing PPG works based on various parameters. (a) PPG works with integrated (on-chip) PD and external (off-chip) PD. (b) PPG works with dc cancellation and without dc cancellation.

system with a small form factor and low power is desired, the on-chip integration of the PD is a promising choice. Fig. 17(b), instead, depicts a spider chart that compares the approaches with and without dc cancellation. It can be seen that high-resolution ADCs and low-noise ones are required if no dc cancellation of the PPG signal is present. On the other hand, when this technique is adopted, the requirements of the ADC are alleviated, making the LDCs smaller and more power efficient. Recent ADC architectures like NS-SAR [83], current-mode variants of NS-SAR [26], [27], and Nyquist rate residue quantization ADCs provide promising alternatives to presently utilized ADC types in the LDC framework. These architectures require shorter conversion times to achieve a comparable DR, thereby enabling lower duty-cycling levels and reducing the overall system power. Additionally, with a shorter conversion time, a more trivial averaging on the DSP side is possible for more precise PPG recording, further enhancing the appeal of these approaches.

Table II summarizes the works on PPG sensor systems reported in the last decade in terms of the various parameters discussed earlier in this review. A further synthesis is reported in Fig. 18, which shows a box chart derived from the performance characteristics of the SoA works included in Table II. A PRF in the range of 1–2048 Hz was employed, while the majority of works reported values higher than 100 Hz. Taking the duty cycle into account (T_{on}), the average is around 1.59% and values as low as 0.0125% [56] (CS) and a maximum of 10% [17] were reported. Almost all of the works have employed aggressive uniform sampling techniques to sample the PPG signals to have such low T_{on} values. On average, a DR of 110 dB was reported; the maximum DR of 136.5 dB was reported by Li et al. [67] and a minimum of around 87 dB by Konijnenburg et al. [86]. It is interesting to note from Fig. 18 that the distribution of DR and SNR values is not as varied as other metrics. This is because of the application-specific requirements imposed on the LDCs. The reported noise performances of these readouts are comparable,

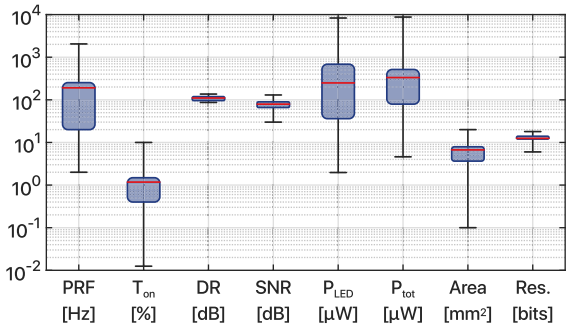

Fig. 18. Box chart summarizing the performance characteristics of SoA PPG works.

resulting in minimal differences in SNR values across SoA works. Lastly, the average power consumption of the LEDs from past works is around 830 μW; the highest reported value is 8.3 mW [12] while the lowest one is 1.97 μW [65].

V. Conclusion

This article presented an overview of different circuit techniques employed in LDCs. The challenges in PPG sensor systems were categorized in macrolevel ones and microlevel ones. At the macrolevel, the complications due to MAs and optical crosstalk that appear as LF noise were discussed. At the microlevel, instead, the power consumption of the LED drivers was identified as a serious challenge, comprising, on average, more than 80% of the total system power consumption. Various sampling techniques like uniform aggressive sampling, CS, and event-driven sampling, employed to mitigate this issue, were analyzed in detail. Moreover, adding to the already existing stockpile of problems, the issue due to the low PI, demanding for high DR in the ADCs present in the LDC, was discussed.

The products with CISs are dominating the consumer electronics market, and even the LDCs have started adopting this technology; thanks to the high QE of these sensors,

a benchmark low power consumption of 4.6 μW was reported [65]. Integrating PD on-chip shows great promise, particularly due to the imperative for miniaturization and seamless integration into wearable PPG devices for commercial purposes. The works with inherent dc and ALR loops demand less SNR than those without, hence making stringent requirements on the part of the ADCs to have a high resolution. Observing the type of ADCs used in the prior LDCs, it is evident that other varieties of ADCs have yet to be explored as 80% of the works employ either a $\Sigma\Delta$ ADC or a SAR one. ADC types like NS-SAR, incremental zoom, and current-mode ones fulfill the requirements for high DR and low power of PPG sensor systems and, therefore, may be considered for exploration in future research in this field. Additionally, LDC architectures devoid of TIA, coupled with faster and low-noise ADCs, could emerge as compelling alternatives to the current SoA schemes. In conclusion, the application areas of PPG monitoring are evolving rapidly; adopting a multimodal sensing strategy by merging various bio-sensing techniques such as ECG, accelerometer data, or temperature sensors presents an intriguing avenue. New application areas have developed like noninvasive glucose sensing [61], skin-cancer diagnostics [89], brain mapping [90], ozone pollutant sensing, and correlated cardiovascular disease monitoring [62]. This generates opportunities for the use of various signal processing and artificial intelligence (AI) techniques for feature extraction of numerous cardiovascular health parameters.

REFERENCES

[1] H. H. Asada, P. Shaltis, A. Reisner, S. Rhee, and R. C. Hutchinson, "Mobile monitoring with wearable photoplethysmographic biosensors," *IEEE Eng. Med. Biol. Mag.*, vol. 22, no. 3, pp. 28–40, May 2003.

[2] P. A. Kyriacou and J. Allen, *Photoplethysmography: Technology, Signal Analysis and Applications*. Cambridge, MA, USA: Academic Press, 2021.

[3] E. Mejia-Mejia, J. Allen, K. Budidha, C. El-Hajj, P. A. Kyriacou, and P. H. Charlton, "Photoplethysmography signal processing and synthesis," in *Photoplethysmography*. Amsterdam, The Netherlands: Elsevier, 2022 pp. 69–146.

[4] P. H. Charlton, P. A. Kyriacou, J. Mant, V. Marozas, P. Chowienczyk, and J. Alastruey, "Wearable photoplethysmography for cardiovascular monitoring," *Proc. IEEE*, vol. 110, no. 3, pp. 355–381, Mar. 2022.

[5] Texas Instruments. (2016). *OPT3002 Light-to-Digital Sensor*. [Online]. Available: https://www.ti.com/lit/gpn/opt3002

[6] AMS-TAOS USA. (2018). *TSL2591 Light-to-Digital Converter*. [Online]. Available: https://eu.mouser.com/pdfDocs/ams_TSL2591.pdf

[7] Renesas Electronics Corporation. (Oct. 2021). *ISL76682 Automotive Grade 4-Channel High Sensitivity Light to Digital Converter With I2C Interface*. [Online]. Available: https://www.renesas.com/us/en/document/dst/isl76682-datasheet?r=1601056

[8] U. Mohammad, M. A. Awan, A. Bermak, and F. Tang, "State-of-the-art light to digital converter circuits applicable in non-invasive health monitoring devices to combat COVID-19 and other respiratory illnesses: A review," *IEEE Sensors J.*, vol. 22, no. 10, pp. 9189–9197, May 2022.

[9] Z. Ebrahimi and B. Gosselin, "Ultralow-power photoplethysmography (PPG) sensors: A methodological review," *IEEE Sensors J.*, vol. 23, no. 15, pp. 16467–16480, Aug. 2023.

[10] P. Schönle, S. Fateh, T. Burger, and Q. Huang, "A power-efficient multi-channel PPG ASIC with 112dB receiver DR for pulse oximetry and NIRS," in *Proc. IEEE Custom Integr. Circuits Conf. (CICC)*, Apr. 2017, pp. 1–4.

[11] A. Sharma et al., "A sub-60-μA multimodal smart biosensing SoC with >80-dB SNR, 35-μA photoplethysmography signal chain," *IEEE J. Solid-State Circuits*, vol. 52, no. 4, pp. 1021–1033, Apr. 2017.

[12] L. Sant, A. Fant, S. Stojanovic, S. Fabbro, and J. L. Ceballos, "A 13.2 b optical proximity sensor system with 130 klx ambient light rejection capable of heart rate and blood oximetry monitoring," *IEEE J. Solid-State Circuits*, vol. 51, no. 7, pp. 1674–1683, Jul. 2016.

[13] E. S. Winokur, T. O'Dwyer, and C. G. Sodini, "A low-power, dual-wavelength photoplethysmogram (PPG) SoC with static and time-varying interferer removal," *IEEE Trans. Biomed. Circuits Syst.*, vol. 9, no. 4, pp. 581–589, Aug. 2015.

[14] S. Song et al., "A 769 μW battery-powered single-chip SoC with BLE for multi-modal vital sign monitoring health patches," *IEEE Trans. Biomed. Circuits Syst.*, vol. 13, no. 6, pp. 1506–1517, Dec. 2019.

[15] Q. Lin et al., "A 119 dB dynamic range charge counting light-to-digital converter for wearable PPG/NIRS monitoring applications," *IEEE Trans. Biomed. Circuits Syst.*, vol. 14, no. 4, pp. 800–810, Aug. 2020.

[16] Q. Lin et al., "A 134 DB dynamic range noise shaping slope light-to-digital converter for wearable chest PPG applications," *IEEE Trans. Biomed. Circuits Syst.*, vol. 15, no. 6, pp. 1224–1235, Dec. 2021.

[17] H.-G. Kim and D.-W. Jee, "A <25 μW CMOS monolithic photoplethysmographic sensor with distributed 1b delta-sigma light-to-digital convertor," in *Proc. 43rd IEEE Eur. Solid State Circuits Conf.*, Sep. 2017, pp. 55–58.

[18] M. Alhawari, N. A. Albelooshi, and M. H. Perrott, "A 0.5 V <4 μW CMOS light-to-digital converter based on a nonuniform quantizer for a photoplethysmographic heart-rate sensor," *IEEE J. Solid-State Circuits*, vol. 49, no. 1, pp. 271–288, Jan. 2014.

[19] F. Marefat, R. Erfani, and P. Mohseni, "A 1-V 8.1-μW PPG-recording front-end with >92-dB DR using light-to-digital conversion with signal-aware DC subtraction and ambient light removal," *IEEE Solid-State Circuits Lett.*, vol. 3, pp. 17–20, 2020.

[20] F. Marefat, R. Erfani, K. L. Kilgore, and P. Mohseni, "A 280 μW, 108 dB DR PPG-readout IC with reconfigurable, 2nd-order, incremental $\Delta\Sigma$M front-end for direct light-to-digital conversion," *IEEE Trans. Biomed. Circuits Syst.*, vol. 14, no. 6, pp. 1183–1194, Dec. 2020.

[21] F. Marefat et al., "A 280 μW 108 dB DR readout IC with wireless capacitive powering using a dual-output regulating rectifier for implantable PPG recording," in *IEEE Int. Solid-State Circuits Conf. (ISSCC) Dig. Tech. Papers*, Feb. 2020, pp. 412–414.

[22] Q. Lin et al., "A 196 μW, reconfigurable light-to-digital converter with 119dB dynamic range, for wearable PPG/NIRS sensors," in *Proc. Symp. VLSI Circuits*, Jun. 2019, pp. 58–59.

[23] Y. Tao and Y. Lian, "A 0.8-V, 1-MS/s, 10-bit SAR ADC for multi-channel neural recording," *IEEE Trans. Circuits Syst. I, Reg. Papers*, vol. 62, no. 2, pp. 366–375, Feb. 2015.

[24] M. Li et al., "A 30-μW 94.7-dB SNDR noise-shaping current-mode direct-to-digital converter using triple-slope quantizer for PPG/NIRS readout," *IEEE J. Solid-State Circuits*, vol. 59, no. 6, pp. 1722–1734, 2024, doi: 10.1109/JSSC.2023.3335068.

[25] A. Aprile, M. Folz, D. Gardino, P. Malcovati, and E. Bonizzoni, "A compact 2.5-nJ energy/conversion NPN-based temperature-to-digital converter with a fully current-mode processing architecture," in *Proc. IEEE 48th Eur. Solid State Circuits Conf. (ESSCIRC)*, Sep. 2022, pp. 473–476.

[26] A. Aprile, M. Folz, D. Gardino, P. Malcovati, and E. Bonizzoni, "A 0.06-mm^2 current-mode noise-shaping SAR based temperature-to-digital converter with a 4.9-nJ energy/conversion," in *Proc. IEEE Custom Integr. Circuits Conf. (CICC)*, Apr. 2023, pp. 1–2.

[27] A. Aprile, M. Folz, D. Gardino, P. Malcovati, and E. Bonizzoni, "An area-efficient smart temperature sensor based on a fully current processing error-feedback noise-shaping SAR ADC in 180-nm CMOS," *IEEE J. Solid-State Circuits*, vol. 59, no. 3, pp. 716–727, Mar. 2024.

[28] T. Seol et al., "A 1 V 136.6dB-DR 4 kHz-BW $\Delta\Sigma$ current-to-digital converter with a truncation-noise-shaped baseline-servo-loop in 0.18 μm CMOS," in *IEEE Int. Solid-State Circuits Conf. (ISSCC) Dig. Tech. Papers*, Feb. 2023, pp. 482–484.

[29] K. Budidha and P. A. Kyriacou, "In vivo investigation of ear canal pulse oximetry during hypothermia," *J. Clin. Monitor. Comput.*, vol. 32, no. 1, pp. 97–107, Feb. 2018.

[30] J. Park, H. S. Seok, S.-S. Kim, and H. Shin, "Photoplethysmogram analysis and applications: An integrative review," *Frontiers Physiol.*, vol. 12, Mar. 2022, Art. no. 808451.

[31] S. Li, L. Liu, J. Wu, B. Tang, and D. Li, "Comparison and noise suppression of the transmitted and reflected photoplethysmography signals," *BioMed Res. Int.*, vol. 2018, pp. 1–9, Sep. 2018.

[32] A. Kamal, J. Harness, G. Irving, and A. Mearns, "Skin photoplethysmography—A review," *Comput. Methods Programs Biomed.*, vol. 28, no. 4, pp. 257–269, 1989.

[33] L.-G. Lindberg, "Optical properties of blood in motion," *Opt. Eng.*, vol. 32, no. 2, pp. 253–257, 1993.

[34] J. de Trefford and K. Lafferty, "What does photoplethysmography measure?" *Med. Biol. Eng. Comput.*, vol. 22, no. 5, pp. 479–480, Sep. 1984.

[35] V. Hartmann, H. Liu, F. Chen, Q. Qiu, S. Hughes, and D. Zheng, "Quantitative comparison of photoplethysmographic waveform characteristics: Effect of measurement site," *Frontiers Physiol.*, vol. 10, p. 198, Mar. 2019.

[36] P. A. Payne, "Measurement of properties and function of skin," *Clin. Phys. Physiological Meas.*, vol. 12, no. 2, pp. 105–129, May 1991.

[37] R. Anderson, J. Hu, J. Parrish, R. Marks, and P. Payne, "Bioengineering and the skin," Eur. Soc. Dermatolog. Res. Symp., Cardiff, U.K., Tech. Rep., 1981, doi: 10.1007/978-94-009-7310-7.

[38] J. Liu, B. P.-Y. Yan, W.-X. Dai, X.-R. Ding, Y.-T. Zhang, and N. Zhao, "Multi-wavelength photoplethysmography method for skin arterial pulse extraction," *Biomed. Opt. Exp.*, vol. 7, no. 10, pp. 4313–4326, 2016.

[39] M. A. Pimentel, P. H. Charlton, and D. A. Clifton, "Probabilistic estimation of respiratory rate from wearable sensors," in *Wearable Electronics Sensors*. Cham, Switzerland: Springer, 2015, pp. 241–262, doi: 10.1007/978-3-319-18191-2_10.

[40] H. Yuan, S. F. Memon, T. Newe, E. Lewis, and G. Leen, "Motion artefact minimization from photoplethysmography based non-invasive hemoglobin sensor based on an envelope filtering algorithm," *Measurement*, vol. 115, pp. 288–298, Feb. 2018.

[41] M. J. Butler, J. A. Crowe, B. R. Hayes-Gill, and P. I. Rodmell, "Motion limitations of non-contact photoplethysmography due to the optical and topological properties of skin," *Physiological Meas.*, vol. 37, no. 5, pp. 27–37, May 2016.

[42] H. Han, M.-J. Kim, and J. Kim, "Development of real-time motion artifact reduction algorithm for a wearable photoplethysmography," in *Proc. 29th Annu. Int. Conf. IEEE Eng. Med. Biol. Soc.*, Aug. 2007, pp. 1538–1541.

[43] G. H. Lee et al., "Stretchable PPG sensor with light polarization for physical activity-permissible monitoring," *Sci. Adv.*, vol. 8, no. 15, Apr. 2022, Art. no. eabm3622.

[44] Y. Zhang et al., "Motion artifact reduction for wrist-worn photoplethysmograph sensors based on different wavelengths," *Sensors*, vol. 19, no. 3, p. 673, Feb. 2019.

[45] R. K. Pandey and P. C.-P. Chao, "A dual-channel PPG readout system with motion-tolerant adaptability for OLED-OPD sensors," *IEEE Trans. Biomed. Circuits Syst.*, vol. 16, no. 1, pp. 36–51, Feb. 2022.

[46] A. Wong, K.-P. Pun, Y.-T. Zhang, and K. Hung, "A near-infrared heart rate measurement IC with very low cutoff frequency using current steering technique," *IEEE Trans. Circuits Syst. I, Reg. Papers*, vol. 52, no. 12, pp. 2642–2647, Dec. 2005.

[47] J. Fine et al., "Sources of inaccuracy in photoplethysmography for continuous cardiovascular monitoring," *Biosensors*, vol. 11, no. 4, p. 126, Apr. 2021.

[48] A. C. Ralston, R. K. Webb, and W. B. Runciman, "Potential errors in pulse oximetry," *Anaesthesia*, vol. 46, no. 3, pp. 202–206, Mar. 1991.

[49] L. Wang, B. P. Lo, and G.-Z. Yang, "Multichannel reflective PPG earpiece sensor with passive motion cancellation," *IEEE Trans. Biomed. Circuits Syst.*, vol. 1, no. 4, pp. 235–241, Dec. 2007.

[50] J. A. C. Patterson, D. C. McIlwraith, and G.-Z. Yang, "A flexible, low noise reflective PPG sensor platform for ear-worn heart rate monitoring," in *Proc. 6th Int. Workshop Wearable Implant. Body Sensor Netw.*, Jun. 2009, pp. 286–291.

[51] A. K. Y. Wong, K. N. Leung, K.-P. Pun, and Y.-T. Zhang, "A 0.5-Hz high-pass cutoff dual-loop transimpedance amplifier for wearable NIR sensing device," *IEEE Trans. Circuits Syst. II, Exp. Briefs*, vol. 57, no. 7, pp. 531–535, Jul. 2010.

[52] P. H. Charlton et al., "The 2023 wearable photoplethysmography roadmap," *Physiological Meas.*, vol. 44, Nov. 2023, Art. no. 111001.

[53] A. Fawzy et al., "Racial and ethnic discrepancy in pulse oximetry and delayed identification of treatment eligibility among patients with COVID-19," *JAMA Intern Med.*, vol. 182, no. 7, pp. 730–738, 2022.

[54] Q. Yousef, M. B. I. Reaz, and M. A. M. Ali, "The analysis of PPG morphology: Investigating the effects of aging on arterial compliance," *Meas. Sci. Rev.*, vol. 12, no. 6, pp. 266–271, Jan. 2012.

[55] M. Elgendi, Y. Liang, and R. Ward, "Toward generating more diagnostic features from photoplethysmogram waveforms," *Diseases*, vol. 6, no. 1, p. 20, Mar. 2018.

[56] V. R. Pamula et al., "A 172 μW compressively sampled photoplethysmographic (PPG) readout ASIC with heart rate estimation directly from compressively sampled data," *IEEE Trans. Biomed. Circuits Syst.*, vol. 11, no. 3, pp. 487–496, Jun. 2017.

[57] S. F. Alamouti, J. Jan, C. Yalcin, J. Ting, A. C. Arias, and R. Müller, "A sparse sampling sensor front-end IC for low power continuous SpO_2 & HR monitoring," *IEEE Trans. Biomed. Circuits Syst.*, vol. 16, no. 6, pp. 997–1007, Dec. 2022.

[58] H. L. Bishop, P. Wang, and B. H. Calhoun, "Application-driven model of a PPG sensing modality for the informed design of self-powered, wearable healthcare systems," in *Proc. IEEE Int. Symp. Circuits Syst. (ISCAS)*, Oct. 2020, pp. 1–5.

[59] V. R. Pamula, M. Verhelst, C. Van Hoof, and R. F. Yazicioglu, "A novel feature extraction algorithm for on the sensor node processing of compressive sampled photoplethysmography signals," in *Proc. IEEE SENSORS*, Nov. 2015, pp. 1–4.

[60] J. Xu et al., "A 665 μW silicon photomultiplier-based NIRS/EEG/EIT monitoring ASIC for wearable functional brain imaging," in *IEEE Int. Solid-State Circuits Conf. (ISSCC) Dig. Tech. Papers*, Feb. 2018, pp. 294–296.

[61] A. Hina and W. Saadeh, "A 186 μW photoplethysmography-based noninvasive glucose sensing SoC," *IEEE Sensors J.*, vol. 22, no. 14, pp. 14185–14195, Jul. 2022.

[62] R. Agarwala, P. Wang, H. L. Bishop, A. Dissanayake, and B. H. Calhoun, "A 0.6 V 785-nW multimodal sensor interface IC for ozone pollutant sensing and correlated cardiovascular disease monitoring," *IEEE J. Solid-State Circuits*, vol. 56, no. 4, pp. 1058–1070, Apr. 2021.

[63] Y. Lee et al., "A 141 μW sensor SoC on OLED/OPD substrate for SpO^2/ExG monitoring sticker," in *IEEE Int. Solid-State Circuits Conf. (ISSCC) Dig. Tech. Papers*, Feb. 2016, pp. 384–385.

[64] B. Lin, Z. Ma, M. Atef, L. Ying, and G. Wang, "Low-power high-sensitivity photoplethysmography sensor for wearable health monitoring system," *IEEE Sensors J.*, vol. 21, no. 14, pp. 16141–16151, Jul. 2021.

[65] A. Caizzone, A. Boukhayma, and C. Enz, "A 2.6 μW monolithic CMOS photoplethysmographic sensor operating with 2 μW LED power," in *IEEE Int. Solid-State Circuits Conf. (ISSCC) Dig. Tech. Papers*, 2019, pp. 290–291.

[66] S. Minto, A. Saadeh, and W. Saadeh, "A 171 μW PPG-based vitals monitoring SoC for asthmatic patients," in *Proc. IEEE Biomed. Circuits Syst. Conf. (BioCAS)*, Oct. 2022, pp. 168–172.

[67] M. Li et al., "A 1.8 V 16 μA 136.5dB DR PPG/NIRS recording IC using noise shaping triple slope light to digital converter," in *Proc. IEEE Custom Integr. Circuits Conf. (CICC)*, Apr. 2023, pp. 1–2.

[68] Y.-S. Shu et al., "A 4.5 mm^2 multimodal biosensing SoC for PPG, ECG, BIOZ and GSR acquisition in consumer wearable devices," in *IEEE Int. Solid-State Circuits Conf. (ISSCC) Dig. Tech. Papers*, Feb. 2020, pp. 400–402.

[69] S. Kim, S. Ko, and D. Jee, "A pixelated monolithic CMOS PPG sensor for spatial feature acquisition," *IEEE J. Solid-State Circuits*, vol. 58, no. 3, pp. 817–826, Mar. 2023.

[70] A. Pedrana, D. Comotti, V. Re, and G. Traversi, "Development of a wearable in-ear PPG system for continuous monitoring," *IEEE Sensors J.*, vol. 20, no. 23, pp. 14482–14490, Dec. 2020.

[71] Y. H. Du, C. Sun, M. Zhang, and S. Mai, "Design of a two-channel forehead PPG sensor," in *Proc. IEEE Biomed. Circuits Syst. Conf. (BioCAS)*, Oct. 2023, pp. 1–5.

[72] Q. Lin, W. Sijbers, C. Avidikou, C. Van Hoof, F. Tavernier, and N. Van Helleputte, "Photoplethysmography (PPG) sensor circuit design techniques," in *Proc. IEEE Custom Integr. Circuits Conf. (CICC)*, Apr. 2022, pp. 1–8.

[73] K. N. Glaros and E. M. Drakakis, "A sub-mW fully-integrated pulse oximeter front-end," *IEEE Trans. Biomed. Circuits Syst.*, vol. 7, no. 3, pp. 363–375, Jun. 2013.

[74] A. Caizzone, A. Boukhayma, and C. Enz, "AC/DC ratio enhancement in photoplethysmography using a pinned photodiode," *IEEE Electron Device Lett.*, vol. 40, no. 11, pp. 1828–1831, Nov. 2019.

[75] A. Caizzone, A. Boukhayma, and C. Enz, "Comprehensive noise analysis in PPG read-out chains," in *Proc. Int. Conf. Noise Fluctuations (ICNF)*, Jun. 2017, pp. 1–4.

[76] C. Enz and A. Boukhayma, "Recent trends in low-frequency noise reduction techniques for integrated circuits," in *Proc. Int. Conf. Noise Fluctuations (ICNF)*, Jun. 2015, pp. 1–6.

[77] S. Fusetto, A. Aprile, P. Malcovati, and E. Bonizzoni, "Readout IC architectures and strategies for uncooled micro-bolometers infrared focal plane arrays: A review," *Sensors*, vol. 23, no. 5, p. 2727, Mar. 2023.

[78] J. Lee, D. Jang, S. Park, and S. Cho, "A low-power photoplethysmogram-based heart rate sensor using heartbeat locked loop," *IEEE Trans. Biomed. Circuits Syst.*, vol. 12, no. 6, pp. 1220–1229, Dec. 2018.

[79] Texas Instruments. *AFE4400 Integrated Analog Front-End for Heart Rate Monitors and Low-Cost Pulse Oximeters (Datasheet)*. Accessed: Jan. 24, 2024. [Online]. Available: https://www.ti.com/lit/ds/symlink/afe4400.pdf?ts=1706263003650
[80] R. Capoccia, A. Boukhayma, and C. Enz, "Experimental verification of the impact of analog CMS on CIS readout noise," *IEEE Trans. Circuits Syst. I, Reg. Papers*, vol. 67, no. 3, pp. 774–784, Mar. 2020.
[81] A. Boukhayma, A. Caizzone, R. Capoccia, and C. Enz, "Design and optimization of low power and low light sensor: (Invited)," in *Proc. IEEE Custom Integr. Circuits Conf. (CICC)*, Mar. 2020, pp. 1–8.
[82] S. Pavan, R. Schreier, and G. C. Temes, *Understanding Delta-Sigma Data Converters*. Hoboken, NJ, USA: IEEE Press, 2017, doi: 10.1002/9781119258308.
[83] J. A. Fredenburg and M. P. Flynn, "A 90-MS/s 11-MHz-bandwidth 62-dB SNDR noise-shaping SAR ADC," *IEEE J. Solid-State Circuits*, vol. 47, no. 12, pp. 2898–2904, Dec. 2012.
[84] M. Tambussi, M. Grassi, E. Bonizzoni, and P. Malcovati, "Trade-offs in active and passive NS-SAR ADCs architectures for ultra-low power audio activity detection applications," in *Proc. 18th Conf. Ph.D Res. Microelectron. Electron. (PRIME)*, Jun. 2023, pp. 165–168.
[85] S. Karmakar, B. Gönen, F. Sebastiano, R. van Veldhoven, and K. A. A. Makinwa, "A 280 μW dynamic zoom ADC with 120 dB DR and 118 dB SNDR in 1 kHz BW," *IEEE J. Solid-State Circuits*, vol. 53, no. 12, pp. 3497–3507, Dec. 2018.
[86] M. Konijnenburg et al., "28.4 a battery-powered efficient multi-sensor acquisition system with simultaneous ECG, BIO-Z, GSR, and PPG," in *Proc. IEEE Int. Solid-State Circuits Conf. (ISSCC)*, Jan. 2016, pp. 480–481.
[87] S.-J. Jung et al., "A 400-to-1000 nm 24 μW monolithic PPG sensor with 0.3A/W spectral responsivity for miniature wearables," in *IEEE Int. Solid-State Circuits Conf. (ISSCC) Dig. Tech. Papers*, Feb. 2021, pp. 1–3.
[88] A. Aprile, E. Bonizzoni, and P. Malcovati, "Temperature-to-digital converters' evolution, trends and techniques across the last two decades: A review," *Micromachines*, vol. 13, no. 11, p. 2025, Nov. 2022.
[89] I. Bodén, "Near infrared and skin impedance spectroscopic in vivo measurements on human skin: Development of a diagnostic tool for skin cancer," Umeå Universitet, Umeå, Sweden, Tech. Rep., 2011, p. 51.
[90] A. T. Eggebrecht et al., "Mapping distributed brain function and networks with diffuse optical tomography," *Nature Photon.*, vol. 8, no. 6, pp. 448–454, Jun. 2014.

Nishan Chettri (Graduate Student Member, IEEE) was born in Darjeeling, India, in 1997. He received the master's degree in electronic engineering from the University of Pavia, Pavia, Italy, in 2023, where he is currently pursuing the Ph.D. degree with the Integrated Microsystems and Sensors (IMS^2) Laboratory, Department of Electrical, Computer and Biomedical Engineering.

His main research interests include data acquisition and readout chains for biomedical sensors.

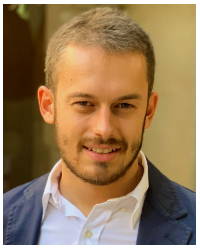

Antonio Aprile (Member, IEEE) was born in Milan, Italy, in 1995. He received the master's (summa cum laude) degree in electronic engineering and the Ph.D. degree in microelectronics from the University of Pavia, Pavia, Italy, in 2019 and 2023, respectively.

He is currently a Postdoctoral Research Fellow with the Integrated Microsystems and Sensors (IMS^2) Laboratory, Department of Electrical, Computer and Biomedical Engineering, University of Pavia. His main research interests include the design and testing of smart temperature sensors, high-resolution current-sensing systems, oversampled ADCs, infrared focal plane arrays (IRFPAs), gigasample-rate DACs, and GaN integrated circuits.

Edoardo Bonizzoni (Senior Member, IEEE) received the Laurea (summa cum laude) degree in electronic engineering and the Ph.D. degree in electronic, computer, and electrical engineering from the University of Pavia, Pavia, Italy, in 2002 and 2006, respectively.

He is currently an Associate Professor with the Department of Electrical, Computer and Biomedical Engineering, University of Pavia. His current research interests include the design and testing of A/D converters, dc–dc converters, high-precision amplifiers, and sensors interfaces.

Dr. Bonizzoni is a TPC Member of IEEE CICC. From 2016 to 2019, he was an Associate Editor of IEEE TRANSACTIONS ON CIRCUITS AND SYSTEMS I—REGULAR PAPERS. Currently, he is the Editor-in-Chief of IEEE TRANSACTIONS ON CIRCUITS AND SYSTEMS II—EXPRESS BRIEFS.

Piero Malcovati (Senior Member, IEEE) received the Laurea degree in electronic engineering from the University of Pavia, Pavia, Italy, in 1991, and the Ph.D. degree in electrical engineering from ETH Zurich, Zurich, Switzerland, in 1996.

From 1996 to 2001, he was an Assistant Professor with the Department of Electrical, Computer and Biomedical Engineering, University of Pavia. From 2002 to 2017, he was an Associate Professor with the Department of Electrical, Computer and Biomedical Engineering, University of Pavia. Since 2017, he has been a Full Professor with the University of Pavia. His research interests include microsensor interface circuits, power electronics circuits, and high-performance data converters.

Dr. Malcovati is a Technical Program Committee Member of several international conferences, including ISSCC, ESSCIRC, SENSORS, ICECS, and PRIME. He is also an Associate Editor of IEEE JOURNAL OF SOLID-STATE CIRCUITS.

Open Access funding provided by 'Università degli Studi di Pavia' within the CRUI CARE Agreement